Nanoparticle Surfaces

DOI: 10.1002/ange.201405043

Revealing the Distribution of the Atoms within Individual Bimetallic Catalyst Nanoparticles**

Peter Felfer, Paul Benndorf, Anthony Masters, Thomas Maschmeyer, and Julie M. Cairney*

Abstract: *To be able to correlate the catalytic properties of nanoparticles with their structure, detailed knowledge about their make-up on the atomic level is required. Herein, we demonstrate how atom-probe tomography (APT) can be used to quantitatively determine the three-dimensional distribution of atoms within a Au@Ag nanoparticle with near-atomic resolution. We reveal that the elements are not evenly distributed across the surface and that this distribution is related to the surface morphology and residues from the particle synthesis.*

From sunscreen to optoelectronics, sensors, catalysis and drug delivery, nanometer-scale particles play an important role in a rapidly growing range of applications. An important example of the commercial application of nanoparticles is nanoscopic catalytic structures, often oxide-supported metal particles. By maximizing the surface area of catalytic metals through the use of nanoparticles, catalytic reactivity can be greatly enhanced and the selectivity strongly influenced. Bi- or multimetallic particles offer even greater scope for fine-tuning.

To better understand their catalytic performance, a detailed understanding of the size, shape, composition and, most importantly, the arrangement of atoms within and on the surface of the particles must be gained. While some atomic-scale information on the structure of nanoparticles has long been accessible through electron microscopy (recently reviewed by Zečević et al.[1]), it has not been generally possible to identify the chemical nature of the individual atoms, meaning that little quantitative, experimental data are presently available as to the precise 3D location of atoms within particles less than 100 nm in size.

Atom-probe tomography (APT) is a microscopy technique that provides three-dimensional (3D) maps of the position and atomic number of individual atoms.[2] It is an ideal tool to bridge the gap between experiments carried out on, for example, flat, single-crystal catalytic surfaces in highly controlled environments, and the industrial reality where many different chemical elements are present and catalysts have three-dimensional, highly curved and faceted surfaces. APT is used herein to provide 3D maps of the individual atoms within Au@Ag catalyst nanoparticles[3] extracted directly from a bulk suspension, that is, no special synthetic techniques are necessary, making this approach relevant to standard nanoparticle synthetic procedures. This type of alloy nanoparticle finds great utility in preferential oxidation[4] (PROX, for example, CO in the presence of H_2—a crucial reaction for fuel cells), in plasmonics[5] as well as non-enzymatic glucose biosensors.[6] The long-term aim of this work is to optimize reactivity and tailor selectivity by controlling the spread of reactive sites on the surface.

For APT experiments, the material to be investigated must be shaped into a sharp needle (radius ca. 100 nm). This shape is required to produce an electric field that is strong enough (some 10 s of $V\,nm^{-1}$) to ionize and thus field-evaporate the atoms at the surface of the specimen. The process is triggered by a pulsed laser. Single field-evaporated ions follow well-defined trajectories towards a 2D detector, where their arrival position is recorded. The 3D positions of the atoms in the sample are reconstructed using sequential back-projection of the ion trajectories. The x and y coordinates of the atoms are reconstructed from the 2D detector hit coordinates of the ions and the z coordinates are obtained from the arrival sequence. The chemical identity of each ion (atom) is determined by the time-of-flight (TOF).[2]

APT experiments are usually carried out on samples that were initially larger than the final needle-shaped specimens, so only subtractive sample preparation techniques are needed. However, to conduct atom-probe experiments on nanomaterials, it is highly desirable to embed the particles into a solid matrix that allows for an even field evaporation of the nanomaterial. This methodology has recently been successfully demonstrated for vapor–liquid–solid grown Si nanowires by using Ni as the matrix,[7] where the catalyst facilitating the wire growth and a section of the nanowire underneath it were captured in one experiment. Prior experiments in which nanoparticles were deposited on a substrate without embedding,[8] and in which agglomerates of nanoparticles were lifted out and analyzed[9] yielded data showing partitioning between a core and a shell. However, the fidelity of the data was insufficient for detailed quantitative analysis in terms of the elemental composition and three-dimensional location on the atomic scale.

[*] Dr. P. Benndorf, Prof. A. Masters, Prof. T. Maschmeyer
Lab. for Advanced Catalysis for Sustainability, School of Chemistry
The University of Sydney
Chemistry Building F11, NSW 2006 (Australia)
E-mail: Thomas.maschmeyer@sydney.edu.au
Dr. P. Felfer, Prof. J. M. Cairney
School for Aerospace, Mechanical and Mechatronic Engineering/
Australian Centre for Microscopy and Microanalysis
The University of Sydney
Madsen Building F09, NSW 2006 (Australia)

[**] This work was funded by the Australian Research Council. We acknowledge the facilities, and the scientific and technical assistance, of the Australian Microscopy & Microanalysis Research Facility at the Australian Centre for Microscopy and Microanalysis, The University of Sydney. T.M. thanks the ARC for a Future Fellowship. P.B. thanks the DFG for a research fellowship.

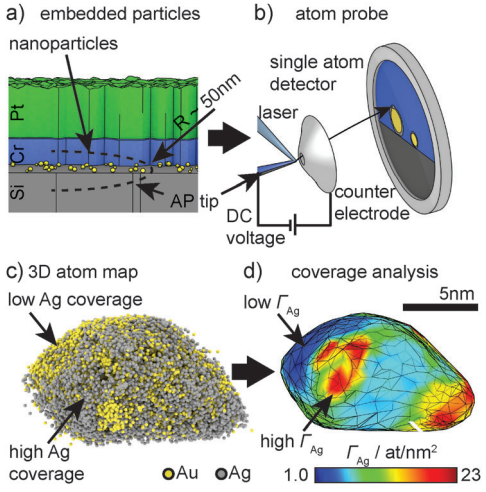

Figure 1. Overview of the atom-probe analysis of nanoparticles. a) Schematic representation of the specimen preparation. The nanoparticles are incorporated in between the Si and Cr layers (see text for details). b) Diagram of a laser atom-probe experiment. c) 3D view of an Au@Ag nanoparticle after sequential reconstruction from 2D detector coordinates and d) quantification of the surface coverage (number of Ag atoms per nm^2).

We have overcome the challenge of producing a strong and dense sample by drying a dispersion of nanoparticles on a Si substrate, and subsequent sputter coating with Cr to provide a stable matrix (Figure 1a). This combination was chosen to minimize the difference in the evaporation fields between the materials. This situation maximizes the resolution by providing a smooth hemispherical tip shape during field evaporation, upon which the 3D tomographic reconstruction is based. The final atom-probe sample, as indicated by the dotted outline in Figure 1a is extracted by using a focused ion beam (FIB) system.[10] The sample is then field evaporated in the atom probe (Figure 1b) and the data processed by a sequential back-projection algorithm[2] to reconstruct a 3D atom map of the particle (Figure 1c, each sphere corresponds to a single atom).

We have estimated an upper limit of the spatial resolution by calculating the distance of each Ag atom to an infinitely thin surface in the 3D map. The distribution of these distance values shows a nearly ideal Gaussian distribution with a full-width-half-maximum (fwhm) of 0.91 nm. Considering that the Ag atoms are, at least in some regions, not present in an ideal monolayer, the actual resolution may be substantially better than the approximately ± 0.5 nm found in this study. A further increase in resolution might be achieved by optimizing sample preparation and reconstruction algorithms.

The 3D data is further analyzed to map the surface coverage of the shell atoms. This coverage corresponds to the number of atoms per unit area of the particle surface, that is, the Gibbsian surface excess Γ, in atoms per nm^2[11] (Figure 1d).

The type of information that can now be obtained for a typical bimetallic particle is displayed in Figure 2. This particle is approximately 15 nm in diameter, consisting of a gold core encased in a silver shell. Figure 2a,b show cross-sectional "slices" extracted from the 3D dataset.

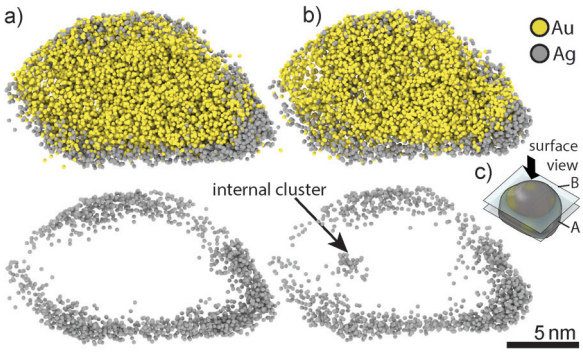

Figure 2. 3D atom maps of 2 nm thick cross-sectional slices of an approximately 15 nm Au@Ag core–shell catalyst nanoparticle. A slice through the thickest part of the particle (a) shows the Ag on the surface. In a slice further up (b), an internal cluster of Ag is also present. In each case, the top image shows core Au and shell Ag atoms, and the bottom image shows the location of just the shell Ag atoms. A sketch of the location of the slices with respect to the surface view is provided in (c).

In these slices, the core and the shell can be resolved easily and variations in the surface coverage are also evident. In the case of Figure 2a, three distinct regions with enriched coverage can be identified. These regions are correlated with areas of higher surface curvature, except for an area on the left of the particle where there is a high curvature region with very little Ag. Along with these enriched and depleted regions, the slice shown in Figure 2b shows an internal cluster of Ag. This is surprising, as the Ag was added after the Au nanoparticles had formed. The observation of internal features was not limited to this particular particle.

For the performance of the nanoparticles, the distribution of the reactive components on the particle surface is crucial. Figure 3a shows this distribution as an atom map, for both the Au and Ag combined, and also for Ag. Remarkably, we are

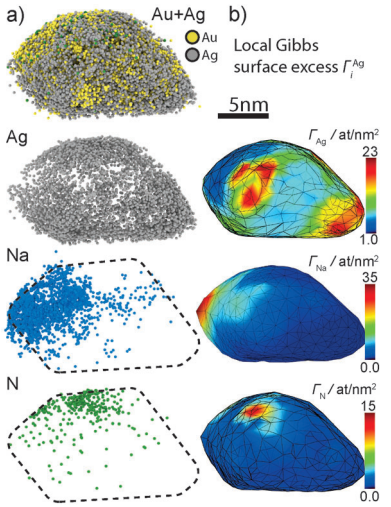

Figure 3. Surface analysis of the Au@Ag nanoparticle shown in Figure 2. The combined atom map (a) shows that the surface coverage of Ag is uneven and that there is a local enrichment of Na and N atoms. b) quantitative maps of the local surface excess of Ag and N atoms (corrected to account for the detector efficiency).

also able to detect Na and N at this resolution and atom maps show their location on the particle's surface. These elements originate from the silver nitrate and the trisodium citrate used in the particle synthesis. Importantly, one observation from these atom maps is that, while Ag is well-dispersed on the particle surface in varying concentrations, Na and N are concentrated in specific areas only. Most of the N is located at just one spot. It is possible that this is a small cluster of AuN on the particle surface, incorporating approximately 450 nitrogen atoms.

To quantify the atomic distributions displayed in Figure 3a, maps of the Gibbsian surface excess of Ag, Na and N were calculated and are shown in Figure 3b. The excess map for Ag shows that the coverage of the particle is patchy, as was the case for all of the nanoparticles examined in this study. Γ_{Ag} varies from approximately 1 at nm^{-2} to approximately 23 at nm^{-2}, that is, from almost no coverage to close to two full monolayers, and is heavily influenced by the presence of Na and N. The coverage of N, Γ_N, varies from 0 to 15 at nm^{-2}, which is close to one monolayer. The Na, occupying an entire edge of the particle, also has a surface excess equivalent to one monolayer in most of the regions where it is found, although a small region with higher excess (up to 35 at nm^{-2}) is present as well.

The interfacial excess maps (Figure 3b) are consistent with the view that there is lower Ag coverage in the regions in which Na and N are observed. To further investigate the validity of this correlation, the Ag excess, Γ_{Ag}, at each datapoint on the specimen surface is plotted against the combined excess of N and Na, Γ_{N+Na} (Figure 4a). This graph shows that, while the amount of Ag found is highly variable in regions with very low or no Γ_{N+Na}, in the regions with higher Γ_{N+Na}, an inverse relationship between Γ_{Ag} and Γ_{N+Na} is evident. That is, less Ag is observed in the regions where more N or Na is present, supporting the correlation.

Figure 3 and Figure 4 also indicate that a relationship exists between the curvature of the specimen surface and the amount of silver present in that region. From an inspection of Figure 3 it appears that high-curvature regions and small facets on the particle surface have a higher density of Ag atoms, whereas a lower Γ_{Ag} is present in regions with lower curvature. To confirm this dependence, Γ_{Ag} is plotted against the mean surface curvature in Figure 4b. To consider solely the effect of curvature, only data where $\Gamma_{N+Na} < 1$ at nm^{-2} was used. The results confirm that there is a strong relationship between surface curvature and the amount of Ag present. Following the Wulff theorem[12] the high-curvature regions and small particle facets are the high-energy surfaces of the Au nanoparticle. As a consequence, Ag which has a lower surface energy than Au,[13] should be attracted to the high-energy surfaces, resulting in a lower energy configuration of the particle. This situation offers possibilities of particle surface tuning by targeting these features synthetically, tuning metal ratios and varying anions (from hard to soft) in the metal precursor salts.

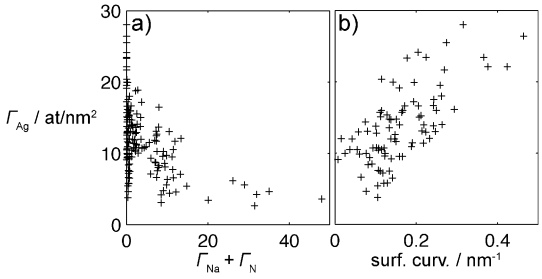

Figure 4. Correlation between Ag surface coverage and surface properties. a) Regions where N and Na are present have less Ag, that is, Ag excess decreases with increasing N + Na excess. b) A correlation between the particle's mean surface curvature and the Ag coverage.

The results shown here have important and far-reaching implications for nanoparticle design. They provide the base for the rational design of (multi)metallic nanoparticles in a way that even allows for the determination of the role and influence of the "spectator species", such as the anions used in the synthesis of the particles. What is their concentration, what is their effect on structural features and eventually performance? How do curvature and general morphological features dictate the assembly of the growing particle? These questions can now be studied and insights exploited to tailor the properties of particles by altering fabrication methods to avoid or encourage adsorption of specific synthetically relevant species, or by producing particles with a specific morphology to rationally generate a spread of the desirable reactive sites.

Experimental Section

For the preparation of the Au@Ag nanoparticles, tetrachloroauric acid ($HAuCl_4 \cdot 3H_2O$; Sigma Aldrich), silver nitrate, and trisodium citrate dihydrate (both Ajax) were used as received. De-ionized water was processed using a Milli-Q (Millipore) Ultrapure Water System. The gold nanoparticles were synthesized according to the following procedure: sodium citrate (20 mg, 0.068 mmol) and tetrachloroauric acid (8 mg, 0.020 mmol) were dissolved in water (40 mL) and heated to 100 °C for 15 min. After 5 min the solution turned dark purple. Sodium citrate (9 mg, 0.031 mmol) in water (2 mL) and silver nitrate (5 mg, 0.029 mmol) in water (2 mL) was added to the gold nanoparticle solution. The reaction mixture was stirred for 2 h at room temperature and 1 h under reflux. The color changed to red/brown.

To prepare specimens for the atom-probe experiments, the Au@Ag nanoparticles in water were dried on a Si substrate and sputter coated with Cr in a Dynavac Xenosput sputter coater. After coating they were transferred into a Zeiss Auriga FIB system, where a strip of Pt was deposited using electron-assisted chemical vapor deposition to provide bulk for the following preparation steps. An FEI Quanta 200 3D FIB instrument was used for sample extraction, where a bar of material is extracted using a micromanipulator, pieces of which are then attached to a support structure.[14] Great care was taken not to introduce any damage from the Ga + focused ion beam, which could impact fine-scale analysis through ion-induced mixing. The ion energies were therefore kept below 10 keV after the lift out.[10] The atom-probe experiments were carried out in a Cameca LEAP 4000X Si instrument[15] (50 K base temperature, using laser-assisted field evaporation, at a pulse frequency of 500 kHz and a pulse energy of 90 pJ).

The data from the atom probe was reconstructed using a standard sequential back-projection algorithm as described in Refs. [2,16]. Additionally, the evaporation voltage evolution, which is used as an estimate for the evolution of the tip radius based on the evaporation field of the sample (33 V nm^{-1}), was smoothed to eliminate voltage fluctuations originating from laser tracking. To increase the fidelity of

the data, each nanoparticle was reconstructed individually. The projection point for the back-projection algorithm was set at the divergence point of the hit density of the nanoparticle that was reconstructed. The data analysis was carried out using custom programs to facilitate interfacial excess mapping, described in Ref. [11].

Received: May 6, 2014
Revised: June 17, 2014
Published online: August 19, 2014

Keywords: atom-probe tomography · heterogeneous catalysts · nanoparticles · silver · surface analysis

[1] J. Zečević, K. P. de Jong, P. E. de Jongh, *COSSMS* **2013**, *17*, 115 – 125.
[2] B. Gault, M. Moody, J. M. Cairney, S. P. Ringer, *Atom Probe Microscopy*, Springer, Heidelberg, **2012**.
[3] J. Turkevich, P. C. Stevenson, J. Hillier, *Discuss. Faraday Soc.* **1951**, *11*, 55 – 75.
[4] X. Liu, A. Wang, X. Yang, T. Zhang, C.-Y. Mou, D.-S. Su, J. Li, *Chem. Mater.* **2008**, *21*, 410 – 418.
[5] V. Pustovalov, W. Fritzsche, *Plasmonics* **2013**, *8*, 983 – 993.
[6] S. Liu, C. Zhang, L. Yuan, J. Bao, W. Tu, M. Han, Z. Dai, *Part. Part. Syst. Charact.* **2013**, *30*, 549 – 556.
[7] O. Moutanabbir, D. Isheim, H. Blumtritt, S. Senz, E. Pippel, D. N. Seidman, *Nature* **2013**, *496*, 78 – 82.
[8] K. Tedsree, T. Li, S. Jones, C. W. A. Chan, K. M. K. Yu, P. A. J. Bagot, E. A. Marquis, G. D. W. Smith, S. C. E. Tsang, *Nat. Nanotechnol.* **2011**, *6*, 302 – 307.
[9] a) Y. Xiang, V. Chitry, P. Liddicoat, P. Felfer, J. Cairney, S. Ringer, N. Kruse, *J. Am. Chem. Soc.* **2013**, *135*, 7114 – 7117; b) D. Isheim, F. J. Stadermann, J. B. Lewis, C. Floss, T. L. Daulton, A. M. Davis, P. R. Heck, M. J. Pellin, M. R. Savina, D. N. Seidman, T. Stephan, *Microsc. Microanal.* **2013**, *19*, 974 – 975.
[10] P. J. Felfer, T. Alam, S. P. Ringer, J. M. Cairney, *Microsc. Res. Tech.* **2012**, *75*, 484 – 491.
[11] P. Felfer, A. Ceguerra, S. Ringer, J. Cairney, *Ultramicroscopy* **2013**, *132*, 100 – 106.
[12] a) G. Wulff, *Z. Kristallogr. Mineral.* **1901**, *43*, 449 – 530; b) C. Herring, *Phys. Rev.* **1951**, *82*, 87 – 93.
[13] W. R. Tyson, W. A. Miller, *Surf. Sci.* **1977**, *62*, 267 – 276.
[14] K. Thompson, D. Lawrence, D. J. Larson, J. D. Olson, T. F. Kelly, B. Gorman, *Ultramicroscopy* **2007**, *107*, 131 – 139.
[15] T. F. Kelly, T. T. Gribb, J. D. Olson, R. L. Martens, J. D. Shepard, S. A. Wiener, T. C. Kunicki, R. M. Ulfig, D. R. Lenz, E. M. Strennen, E. Oltman, J. H. Bunton, D. R. Strait, *Microsc. Microanal.* **2004**, *10*, 373 – 373.
[16] P. Bas, A. Bostel, B. Deconihout, D. Blavette, *Appl. Surf. Sci.* **1995**, *87/88*, 298 – 304.

